Small-Angle Neutron Scattering Studies on the Mesoporous Molecular Sieve MCM-41

Karen J. Edler, Philip A. Reynolds, and John W. White*

Research School of Chemistry, Australian National University, ACT, Australia 0200

Received: May 21, 1997; In Final Form: February 25, 1998

A pure silica MCM-41 preparation with high crystalline order perpendicular to the channels has been examined using small-angle neutron scattering and the contrast variation method in both the calcined and template-containing forms. This defines various structural features such as template and water distributions and content, local silica density, and surface properties. Adsorption isotherm data, NMR, previous neutron scattering data, and the SANS data allow a choice between proposed models for the channel structure of MCM-41, in terms of the straightness of the channels and their surface roughness.

Introduction

The silicate molecular sieve MCM-41 appears, from electron microscopy, to be composed of linear mesoporous channels that form a hexagonal close-packed array in a matrix of amorphous silica.[1,2] It is formed by the condensation of a silicate shell around a surfactant liquid-crystal template. The channel arrangement and structure of the silicate in the walls are of interest as it will affect the catalytic and adsorptive properties of the material. The present paper is concerned with differentiating by small-angle neutron scattering between two models of the two-dimensional projection of the wall structure onto the basal plane for a specially prepared material exhibiting seven orders of diffraction in the basal plane. Our preferred model is derived primarily from the form factor of synchrotron X-ray diffraction data[3] together with information from neutron diffraction and inelastic neutron scattering from hydrogen adsorbed on MCM-41 at low temperatures.[4] It differs significantly from the conventionally assumed smooth walled linear channels passing through silica of essentially bulk density. In further discussion we mean by "smooth", at this almost molecular scale, a surface on which the adsorption of small molecules ranging in size from dihydrogen to neopentane give the same specific surface area.[4]

The best fit to the X-ray data postulates that the basal plane projection of the structure has two distinct regions of silica density, around a "through channel" of smaller radius than previously assumed (see Figure 1, numbers are typical of various samples[3]). The data only allow us to speak of the projected structure, but this is consistent with either straight sided, cylindrical channels lined with a more diffuse form of silica or channels with smooth walls but with a diameter or central position modulated along their length. In projection, there is a continuous wall of silica (density 0.99 g cm^{-3}—about half that of ordinary colloidal silica) surrounding the mesopore channels and a lower density (0.87 g cm^{-3}) silica region of thickness 12 Å between this and the cylindrical holes, which have radii of only around 7 Å.[3] The errors on these estimates ca. 4−5% in absolute density and less than 1% between the regions.[3,4] Thus, the totally open diameter on projection of these samples is much smaller than previously thought, while the walls apparently contain a great deal of void space. This is consistent with the apparent total porosity of the structure to hydrogen gas. There

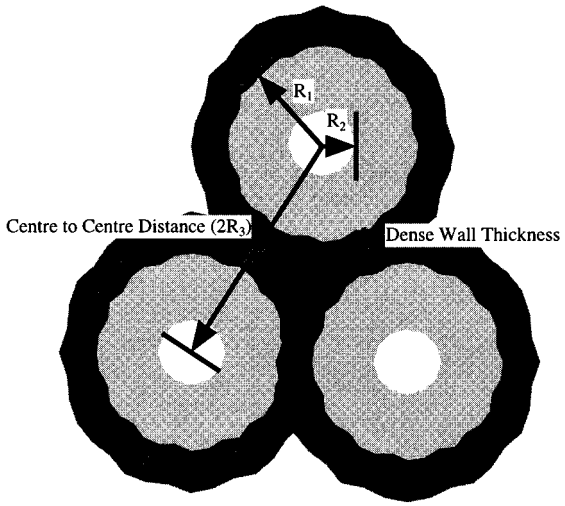

Figure 1. Schematic diagram for the proposed model of MCM-41 in projection onto the basal plane. The two silicate density regions around the hexagonally packed channel are shown with R_2, the hole radius = 7 Å; R_1, the radius to the more dense projection, =21 Å; and $2R_3$, the hexagonal lattice unit cell, =48 Å. The region inside, radius R_2, is called the "central hole"; that between R_2 and R_1 the "lining"; that outside R_1; the rest, the "wall".

are, in projection on the basal plane, three regions differing in electron density in this model. While the data exclude a model with only two density regions, i.e., the conventional "wall/hole" model, other more complex density arrangements may fit equally well. The diffraction from CM-41 with adsorbed hydrogen at different loadings provides further support for the more complex model. Other workers have found similarly low wall densities for CM-41 materials (e.g., 0.97(4) g cm^{-3} for boron-substituted CM-41[5]); however, they have not discussed the detailed structure of the walls. We have quoted "densities" for walls since, in projection, we are averaging over a substantial volume of material; a density based on volumes of a few hundred $Å^3$ would not of course be meaningful.

However, any such more complex structure is constrained by results from other techniques. ^{29}Si MAS NMR,[6,7] wide angle neutron diffraction,[8] and adsorption isotherms[4,9−12] imply a relatively smooth silica surface, with the silica locally resembling bulk silica. Given that our model, in projection, intimately

* Author for correspondence.

S1089-5647(97)01694-5 CCC: $15.00
Published on Web 04/17/1998

mixes void space and silica, it is valuable to provide a further independent test.

Small-angle neutron scattering (SANS) provides this test of the proposed model and, in particular, of the template and water positions in the composite structure. The contrast match points determined by the contrast variation method are sensitive to the variations in density and template distribution in the silica−organic material. Furthermore, the large molecular size of the template and its well-known shape allow us to make some further deductions about wall roughness and local channel geometry.

Only a few other SANS studies have been published. Firouzi et al.[13] report one pattern taken in D_2O of a 1 wt % CTAB solution with and without dissolved silica showing the development of a sharp peak from a hexagonal array of rods from the broad peak characteristic of spherical micelles. Auvray et al.[14] published a brief report of a SANS study on the formation of silica gels from TEOS in the presence of *n*-alkylammonium bromide surfactants with different chain lengths. They also show that prior to silicate addition the SANS pattern is typical of disordered isotropic phases containing rodlike micelles. In short-chain surfactant systems (C_8 and C_{12}) upon silica gel formation SANS developed corresponding to a fractal aggregate structure with dimension 1.9, but the scattering remained dominated by micelle interference peaks indicating a system with short-range order but no liquid-crystal structure. For C_{14}, the development of the hexagonal mesophase during gelation was noted.

A more extensive study has been reported by Glinka et al.[15] which also focuses on the synthetic mechanism. They also find that the scattering from calcined samples can be masked by a solution containing 60% D_2O, having the same scattering length density as amorphous silica, and that the calcined samples are fully accessible to water. The power-law scattering for dry calcined materials is reported to have a $Q^{-4.3}$ dependence, characteristic of a rough surface. They found that the masking solutions were not able to penetrate the structure of uncalcined samples, but no further comment on the detailed structure of these materials is made.

We have carried out SANS measurements on MCM-41 synthesis gels at various stages of preparation, as well as on the final calcined products. We will show that the results of these experiments are consistent with the projection of template and silica distribution described above and illustrated diagrammatically in Figure 1. In our analysis we have consistently assumed, and used the nomenclature, that the MCM-41 material consists of large "particles" of MCM-41 whose internal structure is the aforementioned hexagonal array of channels in silica.

Experimental Section

A detailed treatment of the theory of SANS is readily available in many textbooks,[16,17] so only a brief explanation of the background relevant to the experiments discussed here will be given. The modulus of the neutron momentum transfer, Q, is defined as $Q = 4\pi/\lambda \sin\theta$, where 2θ is the scattering angle. Then, the intensity, $I(Q)$, of the resulting scattering is related to the square of the "contrast". The "contrast" is the difference in scattering length density between the particle and the medium. The scattering length density, ρ_n, is given by

$$\rho_n = \frac{\rho N_A \sum b_i}{M_w} \qquad (1)$$

TABLE 1: Scattering Length Densities (ρ_n) for All Components Used in the MCM-41 Preparations Studied

material	ρ_n ($\times 10^{10}$ cm^{-2})	material	ρ_n ($\times 10^{10}$ cm^{-2})
CTAB	−0.244[a]	CH_3COOH	1.046[a]
SiO_2	3.48[11]	H_2O	−0.562[11]
H_2SO_4	2.101[a]	D_2O	6.34[11]
NaOH	1.826[a]	KBr	1.461[a]

[a] Calculated from the atomic scattering lengths and densities of the materials.[34]

where $\sum b_i$ is the summation of the scattering lengths of all nuclei in the scattering medium, ρ is the density of the medium, N_A is Avogadro's number, and M_w is the molecular weight of the scatterer. The variation of scattering length density with changes in isotopic composition of the surrounding solution (H_2O (-0.56×10^{10} cm^{-2}) and D_2O (6.34×10^{10} cm^{-2})[18]) and the template leads to the ability to change the contrast of a solution without significantly varying other properties of the sample.

Uniform particles in a solution that have the same scattering length density as that of the surrounding solution do not contribute to the scattering in a SANS experiment and are said to be contrast matched (i.e., $I(Q) = 0$). We note that particles with an internal structure will still scatter at Q's other than zero but that still $I(Q=0) = 0$. We measure the scattering from a series of samples containing fractions of H_2O and D_2O that bracket the unknown scattering length density for the particles in a solution in order to determine the contrast match point. In the case of MCM-41 the mostly hydrogenous surfactant template has a small and negative, -0.24×10^{10} cm^{-2}, scattering length density quite different from that of silica, 3.48×10^{10} cm^{-2}.[18] This difference in contrast allows conclusions to be drawn about the distribution and relative amounts of surfactant and silica in the composite particles by following the intensity variations. The scattering length densities for all components of the MCM-41 preparations are given in Table 1.

The SANS from three types of samples has been examined: (1) the initial unheated synthesis gels, (2) the initial synthesis gels at various stages after heating, washing, and calcining to produce MCM-41 by the initially published method, and (3) the initial synthesis gels after heating, etc., but following the optimized synthesis method.[19]

The small-angle neutron scattering experiments were carried out on the LOQ small-angle scattering instrument at ISIS at the Rutherford Appleton Laboratory, UK,[20,21] on the SAD instrument at IPNS, at Argonne National Laboratory, Chicago, IL,[22] and on the NG3SANS instrument at the CNRF, NIST, Washington, DC.[23,24] The samples were contained in flat quartz cells (1 mm sample thickness) sealed with Teflon stoppers. All SANS measurements were performed at 25 °C.

The Initial Synthesis Gels. The MCM-41 preparations were made up as previously described[19,25] using sodium silicate solution (~14% NaOH, ~27% SiO_2) from Aldrich, cetyltrimethylammonium bromide (CTAB, 98%) from Fluka, sulfuric acid from Univar (analytical reagent grade, 98%), and D_2O from AEC Canada (99.99%). The synthesis gels were all prepared identically by adding an acidified sodium silicate solution to a cetyltrimethylammonium bromide (CTAB) solution with vigorous stirring. Various amounts of purified H_2O and D_2O were used in making up the acidified sodium silicate solutions and the surfactant template solutions in order to achieve solutions ranging from 0 to 90 mol % D_2O.

A SANS contrast series was obtained from four series of variously deuterated unheated synthesis gels containing 11.5%,

5%, and 2% CTAB (as weight percent of the total preparation mass) as well as for a salted gel containing 4.3% CTAB and 0.2 M KBr.

The small-angle X-ray scattering was also measured for these gels. The first three unsalted gels showed four relatively narrow Bragg peaks associated with a hexagonal lattice, as previously observed. However, the synthesis gel containing 4.3 wt % CTAB and 0.2 M KBr showed highly unusual behavior. It showed only a single MCM-41 Bragg diffraction peak with broad wings at $Q = 0.1394$ Å^{-1} which did not change much with aging. A sample with 11.5 wt % CTAB and 0.4 M KBr never developed any hexagonal MCM-41 peaks at all, showing only the lamellar crystalline CTAB peaks. There is clearly some disruption to the formation of an ordered structure caused by the presence of the salt. We hypothesize that, analogous to the effect of salt on surfactant solutions,[26] the KBr has the effect of disrupting the formation of a hexagonal structure. This is discussed in more detail elsewhere.[27]

MCM-41 by the Method of Beck et al. This first MCM-41 synthesis followed the method published earlier[28] based on the initial paper by Beck et al.[1] These initial preparation gels typically had the molar compositions CTAB 1.00:SiO_2 1.90:Na_2O 0.74:H_2SO_4 0.28:H_2O/D_2O 149. Five solutions, having D_2O concentrations of 0, 30, 50, 70, and 90 mol %, were heated in autoclaves at 100 °C for 3 days, without stirring. These unfiltered wet, heated, synthesis gels were run on a SANS machine, and the series is hereafter referred to as the "ordinary preparation" *heated* synthesis gel.

The wet gel from a second similar preparation series was filtered after heating, and three dried MCM-41 samples were obtained from it. The first of these was a filtered sample that still contained excess template (called *as-prepared*). The second, a filtered sample that had been washed three times in hot water to remove excess template and then dried (called *washed-and-dried*), and finally, a calcined sample (*calcined*), produced by heating in air in a muffle furnace at 500 °C overnight.

SANS contrast series on the two dried MCM-41 materials, washed-and-dried and calcined, were obtained after suspending them in solutions containing D_2O concentrations of 10, 30, 50, 70, and 90 mol %. To ensure no air was trapped in the MCM-41 channels, the samples were evacuated before the aqueous solutions were added to the powders. A dry sample of each of the two series was also run to provide another contrast point, since air has a scattering length density corresponding to a water mixture containing 8.9 mol % D_2O. Neutron scattering patterns from these samples at air contrast are shown in Figure 2. They contain two types of information, as we shall elaborate below. At low Q (<0.05 Å^{-1}) the scattering arises from the whole particle, and we can deduce information related to particle size, composition, and surface texture. At higher Q, around 0.15 Å^{-1}, the Bragg diffraction peak gives information about the internal structure of the particle, that is, the nature and packing of the channels within the particle.

Small-angle X-ray patterns for these materials also clearly show four Bragg diffraction peaks. The lattice d spacing changes from ca. 43.5 Å for the initial synthesis gel to 41.4 Å for the uncalcined material and to 35.8 Å for calcined materials from the same preparation. This contraction on drying, and again on calcination, is probably at least partially due to further silica condensation and physical relaxation of the silica framework as the CTAB and water are removed and has been seen by others.[1,29] The BET surface area calculated from nitrogen adsorption and desorption isotherms for the calcined sample

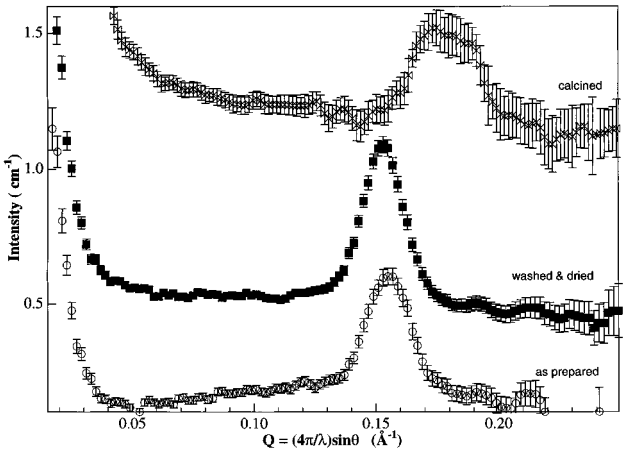

Figure 2. Small-angle scattering patterns at air contrast for the as-prepared, washed, and calcined samples from the ordinary MCM-41 synthesis.

TABLE 2: Surfactant/Silica Ratios (mol/mol) for As-Prepared, Washed-and-Dried, and Calcined Samples from Ordinary and Acid-Titrated MCM-41 Preparations

	acid-titrated preparation	ordinary preparation
as-prepared	0.442	0.349
washed-and-dried	0.153	0.209
calcined	0	0

from this series was 804 m^2 g^{-1}. Small samples of each of the stages of this preparation were calcined to determine gravimetrically the amount of CTAB remaining in each. These surfactant/silica ratios are shown in Table 2 as molar ratios. The ratios for the as-prepared materials are slightly higher than the usual ratio of surfactant to silica in such materials of around 0.33,[29] since they were not as thoroughly washed with water as is usual during the filtration process. The intent here was to avoid washing out any surfactant in the structure and so give an upper bound to the stoichiometry.

MCM-41 by the Method of Ryoo and Kim. A second synthetic method investigated followed the optimized preparation[19] based on the method published by Ryoo and Kim[30] which results in MCM-41 having a much higher degree of long-range order than that obtainable in the ordinary MCM-41 preparation outlined above. The molar composition of the gels for the preparations titrated with acid was typically CTAB 1.00:SiO_2 2.03:Na_2O 0.79:H_2SO_4 0.27:CH_3COOH 0.45:H_2O/D_2O 173. This composition was selected on the basis of earlier studies which showed that this gave the best quality, as measured by X-ray diffraction, final product.[28] Using this method, a synthesis gel contrast series of 0, 30, 50, 70, and 90 mol % D_2O was also prepared. However in this synthesis, after 24 h heating of the start gels at 100 °C, each autoclave was cooled to a comfortable handling temperature and opened, and a titration was performed with 1 M acetic acid (BDH, AnalaR) so as to bring the pH of the whole gel system back to a pH of 11**.** The autoclaves were then resealed and heated for a further 24 h, and the sequence was repeated until 4 days of heating had elapsed. These unfiltered wet, heated, synthesis gels were run on a SANS machine, and the series is hereafter referred to as the "acid titration" heated synthesis gel.

As with the "ordinary preparation", a second preparation was made up and treated to produce as-prepared, washed-and-dried, and calcined samples. A further discussion of the different characteristics of these samples has been give elsewhere.[19]

SANS contrast series of 10, 30, 50, 70, and 90 mol % D_2O were run on the washed-and-dried and calcined series, with the

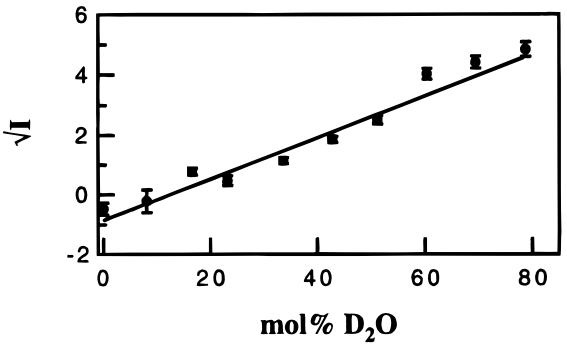

Figure 3. A contrast plot of $\sqrt{I}$ from Porod plots at $Q = 0.015$ Å^{-1} against mol % D_2O in the solvent mixture of H_2O/D_2O for the synthesis gel sample containing 11.5 wt % CTAB.

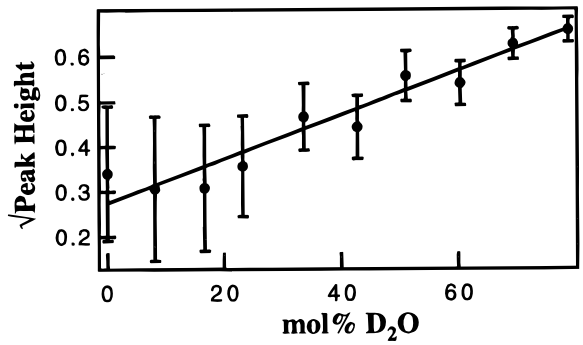

Figure 4. A contrast plot of $\sqrt{}$(peak height) against mol % D_2O in the solvent mixture of H_2O/D_2O for the synthesis gel containing 11.5% CTAB.

air contrast used to provide another contrast point. A contrast series was also run, for comparison, on a second washed, dried MCM-41 sample prepared by the acid titration method but which used H_2SO_4 as the titrant to maintain a constant pH of 10 during the synthesis, as this had been found to produce material with the greatest degree of long-range order. The molar composition of the synthesis gel for this preparation was CTAB 1.00:SiO_2 2.08:Na_2O 0.81:H_2SO_4 0.57:H_2O 166 to give the best quality product.[19]

These samples showed five or six Bragg diffraction peaks in X-ray diffraction using a conventional source. These could be indexed on a hexagonal lattice in the small-angle X-ray scattering pattern. Samples produced using the same method show seven diffraction peaks in X-ray diffraction patterns taken at a synchrotron X-ray source.[3] The samples from the acid-titrated preparations contract less than those from the ordinary preparation upon calcination (from ca. 43.7 Å wet, to 43.5 Å dried, to 41.6 Å calcined), indicating that the silica lattice is already fairly densely polymerized in the initial synthesis gels samples. The BET surface area calculated from nitrogen adsorption and desorption isotherms on the acetic acid-titrated calcined material was 940 m^2 g^{-1} , and for the sulfuric acid-titrated materials it was 880 m^2 g^{-1}. Small samples of each of the stages of this preparation were again calcined to determine gravimetrically the amount of CTAB remaining in each (Table 2).

Obtaining Contrast Match Points. The contrast match point for the whole particle requires the use of the intensity at $Q = 0$. Conventionally, for small particles, this is obtained by extrapolation using a Guinier plot. However, in this case, as we shall show in the section on Porod analysis, the particles are very large. Since all points on the scattering obey a Porod power law and respond to contrast variation in almost the same way, it is possible to obtain the scattering length density difference at the interface between particle and solution from any of the low Q values of the intensity. Again, this is effectively an extrapolation to $Q = 0$. It is fortunate that the particles are not of an intermediate size when extrapolation would be far more difficult. We select a low Q value and plot the square root of the intensity at that value against the concentration of D_2O; the precise Q value does not matter. A typical example (for the ordinary, unheated synthesis gel containing 11.5 wt % CTAB) is shown in Figure 3.

The intensity of the 10 Bragg reflection in the neutron diffraction was also sensitive to the H_2O/D_2O concentration of the preparation. (For a two-dimensional crystal the *hk* nomenclature for the Bragg peak is used.) For the rewetted, template-containing samples this indicates some degree of water penetration into the structure, unlike that noted by Glinka et al.[15]

TABLE 3: Experimental Values for the Contrast Match Points for Intensity Values at Low *Q* and Bragg Peak Intensities of Initial Synthesis Gels Containing Various Amounts of CTAB[a]

CTAB (wt%)	low *Q*	10 peak
11.5	12(2)	−56(28)
5	10(4)	−52(39)
2	14(5)	−180(47)
4.3 + 0.2 M KBr	18(1)	*b*

[a] The contrast match points are given as mol % D_2O, and the errors given are carried through from the errors from least-squares fitting to the data. [b] No peak was observed in this experiment.

TABLE 4: Contrast Match Points for Ordinary and Acid-Titrated MCM-41 Preparations at Various Stages of the Synthesis[a]

	acid preparation		ordinary preparation	
preparation stage	low *Q*	10 peak	low *Q*	10 peak
heated synthesis gel	13(1)	−36(20)	9(2)	−120(13)
washed-and-dried	22(1)[c]	−160(20)[c]	19(1)	−100(6)
	28(1)[d]	−390(28)[d]		
calcined	58(2)	61(4)	61(4)	62(6)

[a] Contrast match points for both intensity values at low *Q* and Bragg peak height are given. Errors are carried through from least-squares fitting of the experimental data. [b] This specimen was not run due to constraints on experimental time. [c] From the acetic acid-titrated preparation. [d] From the sulfuric acid-titrated preparation.

Contrast match points for the 10 diffraction peak therefore were obtained for all samples. These contrast match points were determined from plots of $\sqrt{}$(peak height) versus mol % D_2O, for those samples in which a peak was observed. They generally occurred at different contrast match points to those for the low Q scattering. A diffraction peak height contrast plot is shown in Figure 4. The contrast match points for all of the unheated synthesis gels are given in Table 3. Those for the heated samples, using both the ordinary and acid-titrated MCM-41 synthesis methods, are listed in Table 4.

Results and Discussion

Particle Surface Structure. Electron microscopy[28] shows that calcined MCM-41 materials contain bundles of partially aligned templated tubes tens of microns long and about a micron across. The origin of the small-angle scattering signal is thus an interesting question. One possibility is that only the smallest sizes of the total particle size distribution are sampled in the Q range of the instrument. Another contribution might be that the observed scattering comes in from the scattering length discontinuities at the edges of the bundles and resembles the "crack scattering" observable for highly crazed solids.

TABLE 5: Porod Slopes from Plots of ln *I* versus ln *Q* for MCM-41 Samples at Various Preparation Stages

sample	contrast, mol % D_2O	acid preparation	ordinary preparation
heated synthesis gel	0	3.9(2)	3.1(2)
	20	3.9(5)	3.7(2)
	40	4.05(6)	4.1(1)
	60	4.08(4)	4.07(4)
	80	3.91(2)	4.08(3)
washed and dried	0	4.07(5)	3.13(2)
	10	3.94(4)	2.47(9)
	30	2.5(2)	3.2(2)
	50	3.98(3)	3.21(4)
	70	4.00(4)	3.23(5)
calcined	8.9	3.72(3)	3.29(3)
	10	3.78(4)	*a*
	30	3.67(3)	3.11(4)
	50	3.4(1)	2.99(6)
	70	2.9(1)	*a*
	90	3.56(5)	3.20(4)

[a] These contrasts were not measured due to restrictions on experimental time.

Porod's law states that

$$I(Q) = 2\pi(\Delta\rho)^2 S/Q^n \qquad (2)$$

where $I(Q)$ is the scattered intensity, Q is momentum transfer, and n is the Porod slope, which is related to the nature of the surface of the particles in the scattering medium.[31] S is the surface area, in m^2 of surface per m^3 of material, and $\Delta\rho$ is the scattering length density contrast between the particle and the surrounding medium. For a sharp interface $n = -4$, and Porod's law is a restatement of the more familiar Fresnel's law of reflectivity. The scattering function for the acid-titrated, more highly ordered MCM-41 samples at various contrasts has a Porod slope of around 4 (see Table 5). The slopes are largely independent of the stage in the synthesis at which the samples were taken. These MCM-41 particles must therefore have a smooth surface at inverse length scales between $Q = 0.01$ Å^{-1} and $Q = 0.06$ Å^{-1}, over which the power law is obeyed. That the major contribution to the scattering fits a power law of exponent about -4 eliminates the possibility that we are observing the tail of a size distribution of *particles* that extends to much larger sizes. We are measuring a *surface* at which there is a scattering length discontinuity. The minimum Q that we reach is insufficient to begin to allow the surface scattering components to interfere to define particle sizes and shapes. As we shall see we must, and can, deduce particle sizes indirectly.

At a D_2O content close to the contrast match points for these samples the Porod slopes of -2.5 to -3 are lower. This may indicate a roughness in the surface or an internal structure[17] which is only apparent when the mean density of the particle is matched to the surrounding solution. MCM-41 samples from the ordinary preparation have lower Porod slopes of around -3 to -3.5 at all contrasts which indicates more inhomogeneity in these samples. Again, close to the contrast match points the slope is lower. In all samples at contrasts close to the match points the effect of noise in the scattering patterns is more apparent since the intensity is close to zero. This leads to a greater error in estimating the Porod slopes. A set of Porod plots for various contrasts of an ordinary preparation synthesis gel containing 11.5% CTAB is shown in Figure 5.

The specific surface areas derived from the absolute intensities and the Porod function vary between 0.3 and 6 m^2 per gram of SiO_2 content of the particles. We adopt this measure rather than "per gram of material" so as to compare between materials

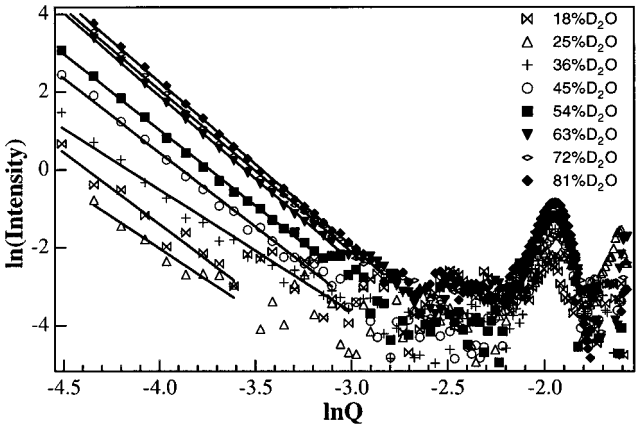

Figure 5. Porod plots of ln *I* versus ln *Q* for the contrast series on an unheated MCM-41 synthesis gel containing 11.5% CTAB.

of different CTAB, water, and air content. These areas are far smaller than the BET surface area for gas adsorption in the calcined materials of about 800 m^2 g^{-1}, indicating that the Porod scattering is indeed from the outer surfaces of the particles containing the hexagonal lattice of channels. If we assume cylindrical particles, then this surface-to-volume ratio implies particles of diameter ca. 5000−100 000 Å. An assumption of other geometries or even a cracked solid gives similar dimensions or lengths for crack-to-crack distances.

The initial start gels, in the region far from contrast, have areas for both types of preparation of 0.3−0.4 mm^2 g^{-1}. On washing the acid preparation sample surface area increases to 1.5 and the ordinary preparation to 6 m^2 g^{-1}. As is reasonable, the washing seems to open up access to water by breaking up joints sealed with CTAB. The ordinary preparation has a higher surface area which correlates with its lesser perfection in diffraction. On calcination the surface areas drop markedly to 1.5 and 1.0 m^2 g^{-1}, respectively. Such a reduction is again reasonable as high-energy silica surfaces anneal together, even at this low temperature compared to the melting point of pure silica.

Evidence from SEM[27] and from a Scherrer analysis of the peak widths of X-ray diffraction data[19] indicates coherence lengths for the hexagonal MCM-41 lattice of the order of 2000 Å. We would expect this length to be some reasonable fraction of the particle size, given that not all "grain boundaries" will be between MCM-41 and air—some will be internal. Given the severe approximations of the Porod theory, this coherence length agrees well with the Porod-derived particle size.

Particle Composition. Contrast Match Points: at Low *Q*. In the calcined materials, for both the ordinary preparation and the acid-titrated preparation, the observed contrast match points for both the peak and low Q at 58−62% are close to both those observed and calculated for amorphous colloidal silica at 61−66 wt % D_2O.[18,32] This indicates that the whole framework is permeable to water as has been found for molecular hydrogen[4] and larger hydrocarbons[5] and that the silica throughout this framework has approximately the same density as ordinary amorphous colloidal silica. There are very few completely enclosed void spaces in the walls, since this would give lower contrast match points than those observed.

The contrast match points for the filtered, washed, and dried samples for both types of preparation are 19−28%. This is markedly lower than for the calcined materials. The structural model of Edler et al.[3] for a highly ordered, washed, dried, and calcined MCM-41 specimen from an acid-titrated preparation has overall 33 vol % silica and 67 vol % void space. Thus,

when the void space in such a sample is completely filled with CTAB, we predict a contrast match point of 22 mol % D_2O. This is not much changed by changes in silica content of a few percent, or inclusion of a few percent of water, but such changes cannot change the CTAB content by more than 10% without affecting the contrast match point noticeably. Thus, the gel particles are by volume broadly $^1/_3$ silica, $^2/_3$ CTAB, and little water. This agrees with the surfactant/silica ratios of Table 2. We shall refine this point when we discuss the Bragg diffraction peak intensities.

The contrast match points at low Q values for all of the ordinary preparation, initial synthesis gels are lower than for the washed-and-dried samples, between 10 and 14 mol % D_2O. The exception is the KBr-containing gel whose value is higher, at 18(1)%, but which forms only a disrupted MCM-41 precursor structure. The low contrast match points in all of these synthesis gels compared to a simple calculation of 22% are probably due to the excess CTAB and various inorganic ions in the liquor. The ionic content of the water regions in the gels raises the actual scattering length density from that predicted simply from H_2O/D_2O ratios, requiring less D_2O at the match point. A simple calculation shows that each 1 mol % of sodium silicate in solution depresses the match point by 0.5%, as measured by H_2O/D_2O. These solutions are concentrated in such ions, so a shift of ca. 10% is easily accomplished by this mechanism. Given the complexity of the reaction mixture, containing many ions as well as excess CTAB, the agreement is satisfactory.

Table 3 shows that the heated synthesis gel samples also have slightly lower contrast match points than expected, at the same values as the unheated gels. Thus, heating has not changed the distribution of material within the gels. The "ordinary preparation" and "acid preparation" systems differ in the quality of their diffraction patterns and their composition as is revealed by scanning electron microscopy (SEM). Micrographs of materials from similar ordinary MCM-41 preparations show large silica spheres coexisting with fibrous MCM-41 material.[28] SEM micrographs of the acid-titrated preparations, which have much greater long-range order (up to seven peaks visible in the SAXS patterns), show no silica spheres.[23] This appears to have no effect on the low Q SANS behavior.

We can summarize these results as showing that the silica structure remains similar, within our uncertainty of about 10%, from initial gels through to calcined materials and differs only in detail between the two preparation methods. It has a density similar to normal amorphous silica, and the large percentage of void space is fully accessible under appropriate conditions to both CTAB and water. We note that the X-ray diffraction does show slight but distinct differences at all stages to which SANS is not so sensitive. Before calcination removes the contents of the void spaces within the siliceous particles, they are at all stages filled with CTAB, to within the accuracy of the low Q SANS scattering. The water and other ions are restricted to the outside of these particles.

Particle Internal Structure. Relative Contrast Variation of the Diffraction Peak and Low *Q* Intensity. The Bragg diffraction peak is more sensitive to the CTAB concentration than the low Q scattering intensity, an indication that the particles have a differentiated internal structure. This sensitivity can be seen from the difference between the absolute intensities of the peak for the calcined and uncalcined samples from the same initial preparation (Figure 2). The negative values for the contrast match point of the peak, observed in all uncalcined MCM-41 samples studied, simply mean that the contrast match point is never reached. It is never possible to include enough H_2O in the silica matrix to match the -0.244×10^{10} cm^{-2} scattering length density of the included CTAB. We note that the change of peak intensity with deuterium content shows that there is indeed water within the MCM-41 particles. If there were no water within the particle, the diffraction peak intensity would not change with water deuteration.

We first consider the conventional model, for our washed-and-dried samples, of a cylinder of CTAB surrounded by silica walls. To obtain both the low Q and the observed diffraction peak contrast match points, with minimum total water content we find that there is 56% CTAB by volume in the channel, while the walls contain 28% SiO_2 and 14% water. Any water in the channel increases the water content of the wall by the same amount and decreases the silica content. These low silica contents are not compatible with free volumes observed in the calcined materials by gas adsorption or with the macroscopic density. Thus, the conventional model is, again,[3,4] found incompatible with a third distinct type of scattering experiment.

If we now turn to our more complex model, we can now model the internal structure of the MCM-41 precursor gel by using a fixed silica density and a structural model derived from our modeling of the X-ray diffraction results upon the uncalcined material.[3] This model describes the observed scattering intensities for Bragg diffraction in terms of the equation

$$I(Q) = \left[(\Delta\rho_1)A_1\frac{2J_1(Q,R_1)}{R_1Q} + (\Delta\rho_2)A_2\frac{2J_1(Q,R_2)}{R_2Q}\mathrm{e}^{-\alpha Q^2}\right]^2 \quad (3)$$

where I is the measured intensity, R_1 (=21 Å) and R_2 (=7 Å) are the radii of the outer and inner cylinders (see Figure 1), A_1 and A_2 are the relative areas of each component, $J_1(Q,R_n)$ is the first-order Bessel function, and α is a Debye−Waller constant. The relative areas, A_1 and A_2, were taken from the X-ray model, and α was likewise set to 1.0 Å^2. The contrasts, $\Delta\rho_1$ and $\Delta\rho_2$, are the differences in scattering length density between the wall and the shell and the shell and the hole, respectively. We have assumed cylindrical structures, but our resolution is insufficient to distinguish more complex cross sections, such as hexagonal.[3] Given the experimental contrast match points, both for the peak and at low Q values, and given the silica content, then the amounts of solvent and surfactant in each part of the structure can be calculated.

An extra term is necessary to describe the scattering at low Q values resulting from the solvent−particle contrast. However, for large particles this contribution is negligible at the first Bragg peak since it decreases steeply with Q, as the Porod plots show. The equation, as given, is for diffraction and concerns only the density fluctuations internal to the particle.

Because the X-ray model was fitted to data from acid-titrated MCM-41 materials only, the calculations were restricted to these materials. However, since the contrast match points for the ordinary preparation MCM-41 materials are generally similar, the conclusions also hold for these materials. For convenience, we have assumed that the partitioning of water into the three components of the structure is isotope-independent.

As expected, modeling the calcined sample gave water concentrations of 100% of all void space in the structure, indicating that the solvent had uniformly penetrated all of the non-silica volume. Attempts to fill this void space with any surfactant gave unphysical results.

The model worked well for those samples that had been removed from their synthesis liquor, i.e., washed-and-dried. A fit of the model to these data indicated high concentrations of CTAB present in the void spaces. The washed-and-dried, acetic

acid preparation sample (contrast match point for the low Q power law region 22(1)mol % D_2O) gave physical values of surfactant and water concentration only when 100% of the central hole (Figure 1) was occupied by CTAB. The wall was ca. 8 vol % water/52 vol % CTAB/40 vol % silica, and the lining (silica-void boundary, whether rough or smooth and meandering) contained negligible water, being ca. 64 vol % CTAB/35 vol % silica. The sulfuric acid-titrated sample with a higher power law contrast match point of 28(1) mol % D_2O gave physical values for the full range of possible concentrations of water and CTAB in the central hole (i.e., 0−100 vol % water) and between ca. 19−50 vol % water/41−10 vol % CTAB/40% silica in the denser walls, while the lining contained ca. 4−30 vol % water/61−35 vol % CTAB/35 vol % silica. These values are highly correlated with one another. Thus, for water concentrations in the central hole higher than 19%, voids in the walls fill with water preferentially to voids in the lining so that if the central hole is 100% water, then the void space in the walls are filled with 50 vol % water and the void spaces in the lining contain only 4 vol % water. An intermediate situation seems more likely than the extremes above—for example, 50 vol % water/50 vol % CTAB in the central hole, 35 vol % water/25 vol % CTAB/40 vol % silica in the walls, and 15 vol % water/50 vol % CTAB/35 vol % silica in the lining.

These values are what would be expected for solvent penetration as the CTAB template is removed from the structure. It is perhaps surprising that the outer silica wall fills with solvent preferentially to the lining. Possibly this indicates the void spaces present in the wall are smaller and are positions of higher energy than those of the lining so that as CTAB is washed out of the structure, protruding CTAB molecules retract into a more uniform micellar configuration closer to the channel center. That the central hole should fill with solvent preferentially to the lining possibly indicates, however, that the lining sites are of lower energy. Overall, the values of the highly negative extrapolated contrast match points for the diffraction peaks arise quite naturally for differentiated CTAB occupancy of void spaces within our model of MCM-41.

The X-ray model can be manipulated to give results for the initial synthesis gel samples, particularly the acid-titrated heated synthesis gel, which would be expected to be the closest in structure to the dried and calcined materials for which the X-ray model was developed. However, the presence of unpolymerized and partially polymerized silica, other ions, excess CTAB partitioned between the MCM-41 phase, solution, the lamellar CTAB crystalline phase, and even large particles of precipitated, amorphous silica allow too many variables in the modeling for this to be worthwhile.

Smooth or Rough Tube Walls. There are two interrelated key questions about the MCM-41 channels which these and our previous experiments raise.[3,4,9−12] First, are the channel walls smooth or very rough, and second how does the center of the channel move relative to the hexagonal unit cell as we move down the channel? We have previously postulated on the basis of X-ray diffraction data two extreme models:[3] (1) a straight channel in which the walls of a narrow channel are lined with a thick layer of finely divided, extremely fluffy, silica; (2) an almost 3-dimensional channel system related to MCM-48 in which the walls of a meandering wide channel are smooth. As a variant of (2), we can postulate (3) a straight channel system in which there are smooth walls but the channel width varies dramatically. The X-ray data and neutron scattering from H_2 adsorbed in MCM-41 exclude (4) the conventional model of straight, wide, smooth walled, cylindrical channels.

The question of roughness can be developed by bringing together some previous observations with those in this paper. Adsorption and desorption isotherms for H_2,[4] N_2,[12] CH_4,[10] CCl_4,[11,12] and CMe_4[9] are all very similar. They, broadly, show BET surface areas of ca. 800 $m^2\ g^{-1}$, very steep capillary condensation after $^1/_3$−$^1/_2$ of the total final adsorption, reversibility, pore volumes derived via the Kelvin equation of ca. 25 Å, and a total adsorption of ca. 0.8 $cm^3\ g^{-1}$. While there are interesting differences of detail, these observations are compatible with a smooth walled wide channel but not with a finely dissected wall. The surface area for a finely dissected wall would be expected to decrease as the molecular size increases, as would the total volume of finally adsorbed material. We would also not expect such steep uniform condensation and agreement with classical ideas for a finely divided wall. The ^{29}Si MAS NMR Q2/Q3/Q4 ratios show that only ca. 9% of the bonds to Si are Si−O−H and 91% are Si−O−Si.[7] This implies relatively massive silica, for example, a double-sided sheet about 13 Å thick. Equally wide angle neutron diffraction from MCM-41 is very similar to that from cristobalite, implying similar local order,[8] again incompatible with very rough walls.

The present experiments show that the initial gels and washed-and-dried samples are essentially only CTAB and silica, the CTAB volume is, for the washed-and-dried acid preparation sample, 0.9 $cm^3\ g^{-1}$, the silica framework density is that of bulk silica (despite the large free volume), and water penetrates all the free volume. CTAB is a much larger molecule than even CMe_4, so the constant accessible volume for the smaller molecules being the same as the total volume of CTAB is good evidence for smoothness of the walls. CTAB aggregations have been much studied, and the headgroup area per molecule is characteristic of the CTAB agglomeration geometry.[33] For planar arrangement we expect 20−30, for cylinders 40−50, and for higher curvatures 60+ $Å^2$ per molecule. In this case given the CTAB content and BET surface area, we deduce a headgroup area of 55 $Å^2$. This implies a cylindrical free volume, possibly with some extra curvature.

Both inelastic and elastic neutron scattering from adsorbed H_2[4] indicate that about $^1/_2$ of the adsorbed molecules in fully filled MCM-41 are attached to the walls. Simple calculations using molecular dimensions derived from bulk density and adsorption measurements show that these fractions are those expected from a smooth surface but are difficult to explain if the surface is highly dissected on the molecular scale. Last, when CMe_4 is adsorbed at almost monolayer coverage, its behavior in the quasielastic neutron scattering region[9] suggests a uniform type of site adsorption, again difficult to reconcile with a rough wall.

Thus we are led to the conclusion that the walls are relatively smooth and that either the channel centroid or the walls themselves move relative to the hexagonal lattice as we move down the channel. This is not inconsistent with electron microscopy by other workers which shows a wide range of slowly curving configurations for the microtubes.[35]

Conclusion

The contrast match points from small-angle neutron scattering experiments give useful information about the structure of MCM-41. They indicate that the calcined material is completely penetrable to water, all voids completely filling. Those parts of the structure that are not penetrable contain silica with the same scattering length density as for amorphous colloidal silica, indicating that the silica structure has much the same density as normal amorphous silica. The contrast match points observed

are not compatible with adsorption experiments if the MCM-41 structure is a simple straight tubular channel surrounded by silica walls. The contrast match points also indicate that in all the uncalcined materials, including the initial synthesis gels, a large part of both the wall and lining volume contain CTAB molecules with a small but significant amount of water and so must be highly porous. However, the CTAB is more easily removed from the silica walls than the silica lining. These results combined with previous work indicate that MCM-41 has a smooth-walled structure but that either or both of the channel walls or centroid moves relative to the hexagonal lattice enough that a smooth-walled and straight channel is a very poor description of the MCM-41 structure.

Acknowledgment. We wish to thank Dr. R. Heenan and Dr. S. King at the Rutherford-Appleton Laboratory, Dr. P. Thiyagarajan at the Argonne National Laboratory, and Dr. T. Slaweki and Dr. B. Hammouda at the National Institute of Standards and Technology for assistance with these experiments. Some of this work has benefited from the use of the Intense Pulsed Neutron Source at Argonne National Laboratory which is funded by the U.S. Department of Energy, BES-Materials Science, under Contract W-31-109-ENG-38. This material is also based upon activities supported by the National Science Foundation under Agreement No. DMR-9423101. We acknowledge the support of the National Institute of Standards and Technology, U.S. Department of Commerce, in providing the neutron research facilities used in some of this work. Travel grants through the Australian Government ISTAC/ANSTO Access to Major Facilities Program are gratefully acknowledged.

References and Notes

(1) Beck, J. S.; Vartuli, J. C.; Roth, W. J.; Leonowicz, M. E.; Kresge, C. T.; Schmitt, K. D.; Chu, C. T.-W.; Olson, D. H.; Sheppard, E. W.; McCullen, S. B.; Higgins, J. B.; Schlenker, J. L. *J. Am. Chem. Soc.* **1992**, *114*, 10834.

(2) Kresge, C. T.; Leonowicz, M. E.; Roth, W. J.; Vartuli, J. C.; Beck, J. S. *Nature* **1992**, *359*, 710.

(3) Edler, K. J.; Reynolds, P. A.; White, J. W.; Cookson, D. *J. Chem. Soc., Faraday Trans.* **1997**, *93*, 199.

(4) Edler, K. J.; Reynolds, P. A.; Branton, P. J.; Trouw, F.; White, J. W. *J. Chem. Soc., Faraday Trans.* **1997**, *93*, 1667.

(5) Marler, B.; Oberhagemann, U.; Vortmann, S.; Gies, H. *Microporous Mater.* **1996**, *6*, 375.

(6) Huo, Q.; Margolese, D. I.; Ciesla, U.; Demuth, D. G.; Feng, P.; Gier, T. E.; Sieger, P.; Firouzi, A.; Chmelka, B. F.; Schuth, F.; Stucky, G. D. *Chem. Mater.* **1994**, *6*, 1176.

(7) Luhmer, M.; Despinose, J. B.; Honnel, H. *Magn. Reson. Imag.* **1996**, *14*, 911.

(8) Fuess, H.; Kirschhock, C.; Pophal, C. *International Union of Crystallography Congress* **1996**, Talk 10.10.01.

(9) Edler, K. J.; Reynolds, P. A.; Branton, P. J.; Trouw, F. R.; Watson, J. N.; White, J. W., unpublished data.

(10) Edler, K. J.; Reynolds, P. A.; Trouw, F.; White, J. W. *Chem. Phys. Lett.* **1996**, *249*, 438.

(11) Branton, P. J.; Reynolds, P. A.; Studer, A.; Sing, K. S. W.; White, J. W. *Adsorption*, in press.

(12) Branton, P. J.; Sing, K. S. W.; White, J. W. *J. Chem. Soc., Faraday Trans.* **1997**, *93*, 2337.

(13) Firouzi, A.; Kumar, D.; Bull, L. M.; Besier, T.; Sieger, P.; Huo, Q.; Walker, S. A.; Zasadzinski, J. A.; Glinka, C.; Nicol, J.; Margolese, D.; Stucky, G. D.; Chmelka, B. F. *Science* **1995**, *267*, 1138.

(14) Auvray, L.; Ayral, A.; Dabadie, T.; Cot, L.; Guizard, C.; Ramsay, J. D. F. *Faraday Discuss.* **1995**, *101*, 235.

(15) Glinka, C. J.; Nicol, J. M.; Stucky, G. D.; Ramli, E.; Margolese, D.; Huo, Q.; Higgins, J. B.; Leonowicz, M. E. *J. Porous Mater.* **1996**, *3*, 93.

(16) Bacon, G. E. *Neutron Diffraction*, 3rd ed.; Oxford University Press: Melbourne, 1975.

(17) Jacrot, B. *Rep. Prog. Phys.* **1976**, *39*, 911.

(18) Iton, L. E.; Trouw, F.; Brun, T. O.; Epperson, J. E.; White, J. W.; Henderson, S. J. *Langmuir* **1992**, *8*, 1045.

(19) Edler, K. J.; White, J. W. *Chem. Mater.* **1997**, *9*, 1226.

(20) Heenan, R.; King, S. In *ISIS User Guide*; Boland, B., Whapham, S., Eds.; ISIS, Rutherford Appleton Laboratory: Didcot, Oxon., U.K., 1992.

(21) Heenan, R. K.; King, S. M. In *International Seminar on Structural Investigations at Pulsed Neutron Sources Proceedings, 1992*; Aksenov, V. L.; Balagurov, A. M., Taran, Y. V., Eds.; Joint Institute for Nuclear Research: Dubna, Russia, 1993; p 176.

(22) Epperson, J. E.; Thiyagarajan, P.; Carpenter, J. M.; Crawford, R. K.; Wozniak, D. G. In *IPNS Progress Report 10th Anniversary Edition*; Rotella, F. J., Ed.; Argonne National Laboratory: Argonne, IL, 1991; p 76.

(23) NIST In *Cold Neutron Research Facility*; National Institute of Standards and Technology: 1996; p 3.

(24) Hammouda, B.; Krueger, S.; Glinka, C. J. *J. Res. Natl. Inst. Stand. Technol.* **1993**, *98*, 31.

(25) Zhao, D.; Goldfarb, D. *J. Chem. Soc., Chem. Commun.* **1995**, 875.

(26) Tiddy, G. J. T. *Phys. Rep.* **1980**, *57*, 1.

(27) Edler, K. J.; Reynolds, P. A.; Brown, A.; Slawecki, T.; White, J. W., manuscript in preparation.

(28) Edler, K. J.; Dougherty, J.; Durand, R.; Iton, L.; Kirton, G.; Lockhart, G.; Wang, Z.; Withers, R.; White, J. W. *Colloids Surf. A* **1995**, *102*, 213.

(29) Chen, C. Y.; Burkett, S. L.; Li, H.-X.; Davis, M. E. *Microporous Mater.* **1993**, *2*, 22.

(30) Ryoo, R.; Kim, J. M. *J. Chem. Soc., Chem. Commun.* **1995**, 711.

(31) Glatter, O.; Kratky, O. *Small-Angle X-ray Scattering*; Academic Press: London, 1982.

(32) Dougherty, J.; Iton, L. E.; White, J. W. *Zeolites* **1995**, *15*, 640.

(33) Israelachvili, J. N.; Mitchell, D. J.; Ninham, B. W. *J. Chem. Soc., Faraday Trans. 2* **1976**, *72*, 1525.

(34) *CRC Handbook of Chemistry and Physics*, 75th ed.; Lide, D. R., Ed.; CRC Press: Boca Raton, FL, 1994.

(35) Aksay, I. A.; Trau, M.; Manne, S.; Honma, I.; Yao, N.; Zhou, L.; Fenter, P.; Eisenberger, P. M.; Gruner, S. M. *Science* **1996,** *273*, 892−898.